DESIGN AND OPERATION OF A CENTRIFUGAL COMPRESSOR IN A HIGH TEMPERATURE HEAT PUMP

Benoît Obert[1]*, Giacomo Persico[2], Paolo Gaetani[2]

[1]Enertime,
1 rue du moulin des bruyères, Courbevoie, France
benoit.obert@enertime.com

[2]Politecnico di Milano, Dipartimento di Energia, Laboratorio di Fluidodinamica delle Macchine
Via Lambruschini 4, I-20156, Milano, Italy

* Corresponding Author

ABSTRACT

This article presents the design, simulation and operation of a single stage 800 kW_e centrifugal compressor operating with HFO R1234ze(E). The compressor is integrated in a high temperature heat pump that converts heat from saturated steam at 48°C into 3.5 MW_{th} of heat at 75°C for a district heating network. The compressor specifications require a high-pressure ratio (above 3), a high isentropic efficiency and a wide operation range.

The compressor design process is discussed in detail, starting from the preliminary optimization based on the mean-line model and then focusing on the aerodynamic design of each component of the compressor. In particular, the design of the inlet guide vanes (IGV), of the impeller, of the vaneless and vaned diffusers, and finally of the exhaust volute are presented in detail. Nominal and off design performances are then assessed by means of computational fluid dynamics (CFD), performed by applying the commercial solver ANSYS CFX. The simulations are based on the two-dimensional Reynolds-Averaged Navier-Stokes (RANS) equations supplemented by a k-ω turbulence model; the thermodynamic properties of the working fluid are modelled by an equation of state based on a Helmoltz free energy approach, implemented as look-up tables in both the design and simulation steps. Preliminary experimental results of a test campaign aimed at partially mapping the compressor performance in terms of pressure ratio, electrical power and rotation speed are presented, and a thorough comparison between experimental data and simulation results concludes the paper. This comparison shows a good accordance between the expected behavior of the compressor and the experimental results: simulated pressure ratios for five different speed lines nearly fall within measurement uncertainties.

1. INTRODUCTION

Heat pumps are systems that transfer thermal energy from a low temperature heat source to a higher temperature heat sink. Their size and thermal power rating vary greatly depending on the application, ranging from a few kW_{th} for domestic heating to several MW_{th} for district and industrial heating (Stoecker, 1998). The heat pump studied in this paper supplies 3.5 MW_{th} at 75°C to a district heating network. The heat source is saturated steam at 48°C coming from the exhaust of a steam turbine that converts waste heat from an incineration plant into power. The relatively low temperature difference between the heat source and the heat sink allows for a high COP (4.3 at nominal conditions) with a simple single compression stage thermodynamic cycle. The working fluid is the low-GWP HFO refrigerant R1234ze(E) (Brown *et al*, 2009).

Together with the heat exchangers and the expansion valve, the compressor is a critical component of the heat pump, and its design is essential to the overall system's performance and availability. The technology chosen for this particular application and commonly used for high power heat pump is a centrifugal compressor. This paper discusses the aerodynamic design of the compressor, its predicted

performance maps and its experimental assessment in the commissioning phase of the heat pump. The design was carried out combining a mean-line code developed in-house at Politecnico di Milano with computational fluid dynamic (CFD) simulations of impeller and diffuser. In this paper, we use the commercial CFD software ANSYS CFX coupled with thermo-physical look-up tables to simulate the compression of the non-ideal fluid inside the compressor. The CFD model of the whole machine is used to predict the nominal and part load performance of the centrifugal compressor, which are eventually compared to experiments performed during the commissioning phase of the heat pump.

The paper is structured as follows. The second section of this work presents the compressor's nominal operating conditions, its main geometrical characteristics and the ones of its components. The design approach is detailed in the third paragraph. The details of the simulation setup and models, the mesh, and the thermo-physical model are provided in the fourth section of this paper. The results of the simulations are then presented in the fifth section and eventually experimental data are compared to the CFD simulations in the sixth and last section.

2. COMPRESSOR CHARACTERISTICS

The compressor is a single stage centrifugal compressor directly overhung on the high-speed shaft of a gear box. The low-speed shaft is coupled to motor equipped with a variable frequency drive (VFD). From inlet to outlet, the compressor is composed of the following elements:

- Variable inlet guide vanes
- An open (unshrouded) impeller
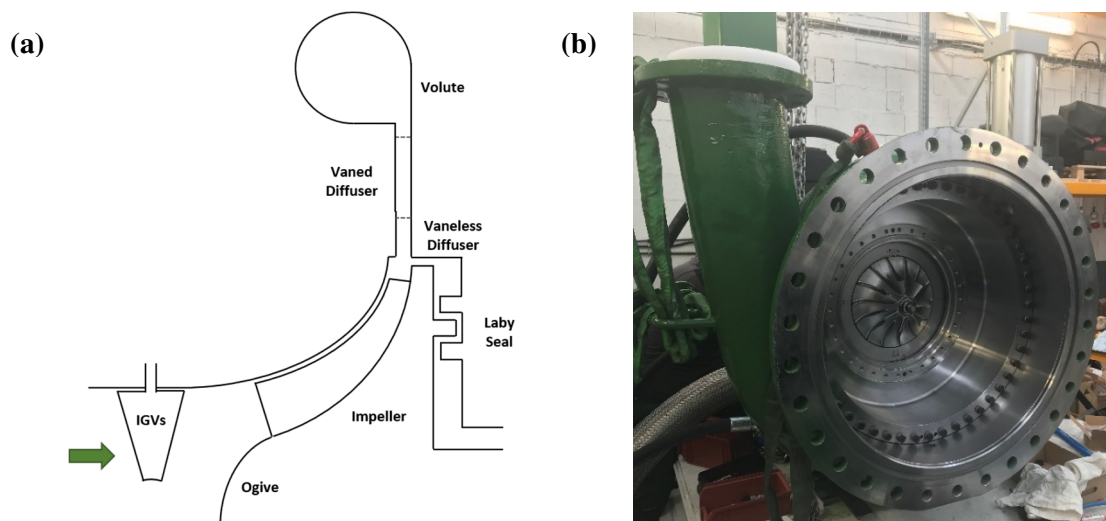- A vaneless diffuser
- A vaned diffuser
- An exhaust volute

Figure 1: (a) Compressor configuration schematic; **(b)** Compressor photo during assembly

Figure 1(a) presents a schematic view of the previously mentioned subcomponents of the compressor. Figure 1(b) is a photo of the compressor during assembly. In this paper, the effect of the variable inlet guide vanes (IGVs) is not studied: the IGVs were kept fully open in both the simulations and the experimental tests.

Table 1 presents the nominal flow conditions of the compressor and some key dimensions, as resulting from the preliminary and aerodynamic design of the machine, which is discussed in the next section. Equations (1) and (2) present formulas for respectively the specific speed and the specific diameter where ω is the rotational speed, D the impeller tip diameter, ΔH is isentropic enthalpy change and $\dot{Q}$ the inlet volumetric flow rate. During the design process (detailed in section 3 of this work), these values are used for compressor technology selection and for attainable isentropic efficiency evaluation (Khan, 1984).

$$\omega_s = \frac{\omega\sqrt{\bar{Q}}}{\Delta H_{is}^{3/4}} \tag{1}$$

$$D_s = \frac{D\,\Delta H_{is}^{1/4}}{\sqrt{\bar{Q}}} \tag{2}$$

Table 1: Compressor characteristics

Nominal Conditions	Value	Unit	Geometrical Characteristics	Value	Unit
Inlet total pressure	7.2	bar	Impeller inlet hub radius	30	mm
Inlet total temperature	39.7	°C	Impeller shroud radius	74	mm
Outlet total pressure	22.4	bar	Impeller tip radius	133.5	mm
Mass flow rate	29.2	kg/s	Vanned diffuser inlet radius	192.5	mm
Rotational speed	13250	rpm	Vanned diffuser outlet radius	310.5	mm
Specific speed	0.71		Diffuser blade height	7.7	mm
Specific diameter	3.63		Volute maximum extension	440	mm

3. COMPRESSOR AERODYNAMIC DESIGN

The first step of the design process was a dimensionless analysis based on the statistical Balje diagram (Balje, 1981). Values of specific speed and specific diameters were chosen to maximize attainable isentropic efficiency under the constraints of mechanical feasibility and manufacturability. The detailed sizing of the machine and of the components was then performed using the in-house mean-line code C-Comprex of Politecnico di Milano, specifically dedicated to centrifugal compressors. C-Comprex features loss and slip-factor correlations specific for centrifugal compressors (Whitfield and Baines, 1990), supplemented by corrections tuned usung experiments performed on the centrifugal compressor installed in the high-speed closed-loop test rig of the Politecnico di Milano (Gaetani *et al.*, 2012). In particular, C-Comprex provided the optimal preliminary design of the impeller, the vaneless diffuser and the volute. The preliminary design of the vaned diffuser was, instead, based on an existing diffuser data base. The detailed shape of the impeller and the diffuser blades were finally determined by means of parametric optimizations based on dedicated CFD simulations of the single blade rows. Key flow conditions and geometrical values for each of the compressor's subcomponents are presented in Table 2.

Table 2: Compressor design details

Quantity		Value	Unit	Quantity		Value	Unit
Impeller inlet	Static pressure	6.6	bar	Vanned Diffuser Inlet	Static pressure	19.0	bar
	Hub flow angle	-35.1	°		Flow angle	71	°
	Tip flow angle	-60.0	°		Mach number	0.74	
Impeller Outlet	Static pressure	14.7	bar	Vanned Diffuser Outlet	Static pressure	22.2	bar
	Mach number	1.1			Blade angle	57	°
	Flow angle	69	°		Area ratio	2.63	

3.1 Impeller
The rotor inlet hub diameter was defined by mechanical constraints and the inlet shroud diameter was set by minimizing the relative Mach number at the blade tip. The impeller is composed of 7 full blades and 7 splitter blades. The rotor outlet section is designed to maximize blade height in order to limit the detrimental effects of the tip clearance. A pinch just downstream of the rotor discharge section was introduced to block the clearance flow reversal and to make the flow at the vaneless diffuser inlet more uniform (Jaatinen-Varri *et al*, 2013). The blade outlet angle of the impeller was refined by resorting to

dedicated 3D CFD simulations of the impeller only, as they revealed that the slip factor had been under-estimated by the mean-line code.

3.2 Diffuser

The vaneless diffuser was designed at constant height and with a radial extension set to match the flow conditions with the vaned diffuser inlet, in particular to avoid the onset of chocked-flow conditions at the inlet of the vaned channel. The flow angle at the inlet of the vaned diffuser was selected so to avoid possible boundary layer separation over a wide operation range and to guarantee a safety margin for diffuser stability. The diffuser blade row is composed of 17 blades, whose profile is a tradeoff between a logarithmic spiral and a straight axis profile. It was optimized parametrically using a 2D CFD model of the blade row.

3.3 Volute

The volute's cross-section and radius evolutions were calculated to match space constraints, downstream piping diameter and minimize total pressure losses.

4. CFD SIMULATION SETUP

CFD simulations of the whole compressor were performed by resorting to a steady RANS 3D model, based on the commercial solver ANSYS CFX 2019 R1. The computational domain (presented in Figure 2(a)) contains the following sub-domains:

- One IGV blade: 325,000 elements structured mesh
- One Impeller full blade and one splitter blade: 1,148,000 elements structured mesh
- Vaneless diffuser and one vanned diffuser blade: 468,000 elements structured mesh
- Volute: 3,326,000 elements unstructured mesh

The number of mesh elements was selected after a grid independence study at the nominal conditions. The heights of the first elements near the wall were set to obtain y^+ values between 30 and 200, thus consistent with the use of wall-functions. The interfaces between stationary and moving parts are modeled as mixing planes. For RANS turbulence closure, we use the k-ω Shear Stress Transport two-equation model. The advection terms in the flow and turbulence equations are discretized with high-resolution schemes (implicit 2nd order bounded schemes), while the diffusive fluxes in the same equations are discretized with central differences. The total temperature and total pressure at the inlet, as well as the static pressure at the outlet are imposed at the domain boundaries. The blade surfaces and the other wetted areas are set as adiabatic no-slip walls. Convergence is attained when the averaged residuals of the mass, momentum, energy and turbulence equations are less than 10^{-5}. The fluid thermo-physical properties are interpolated from a 400 by 400 look-up table that was generated using the Helmholtz free energy equation of state presented in Thol and Lemmon (2016). These tables span over the superheated vapor region of the gas compression.
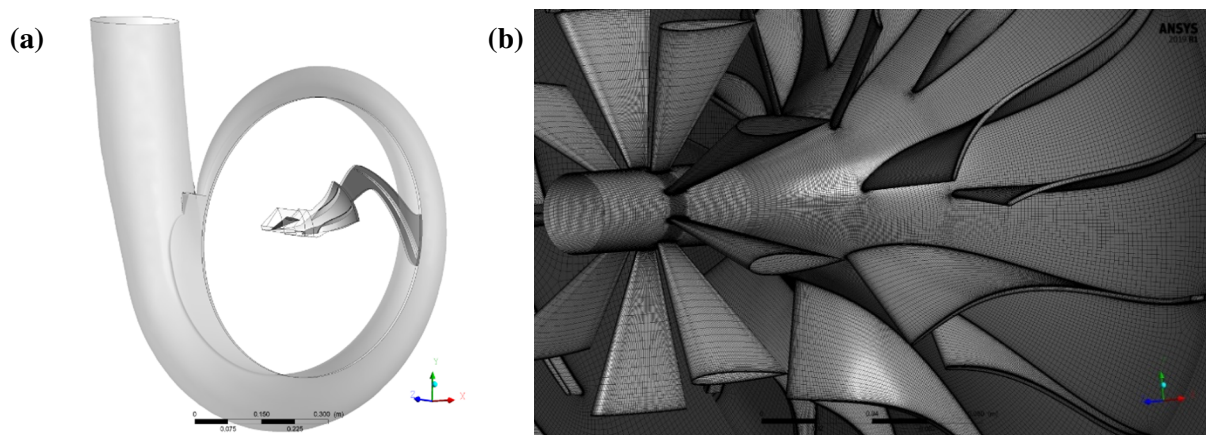
(a)   **(b)**

Figure 2: (a) Computational domain; **(b)** Mesh sample

5. CFD RESULTS

5.1 Nominal Point

CFD calculations were first carried out at the nominal conditions presented in Table 1. The results in terms of relative Mach number are presented in Figure 3. As mentioned in paragraph 3, the initial impeller blade outlet design led to a higher slip factor than expected, the resulted in a high incidence angle at the vaned diffuser leading edge and to a significant flow separation in the diffuser. Consequently, both the impeller and the diffuser were re-designed so to achieve an optimal matching between the two components in the nominal condition, demonstrated by the smooth flow configuration depicted in Figure 3.
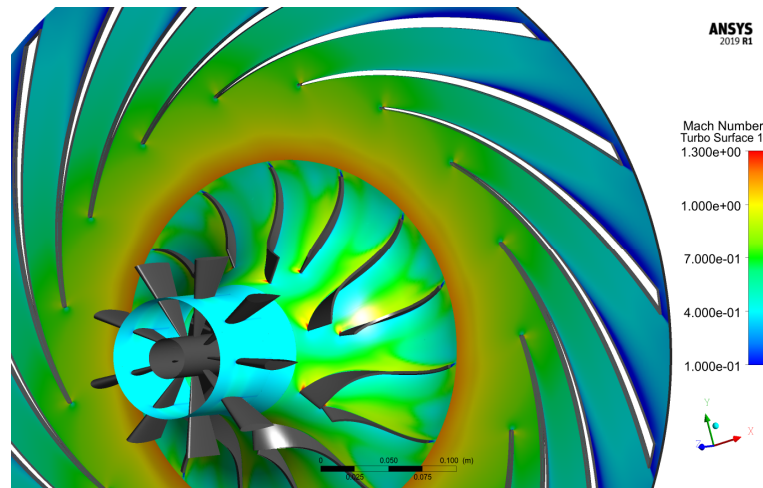

Figure 3: Relative Mach number field at half span

Table 3 reports the CFD result data of key quantities for the analysis of the flow inside the compressor. Average values are computed using mass flow weighted integral averages over a surface of interest.

Table 3: Nominal Conditions CFD results

Quantity		Value	Unit
Impeller	Inlet relative static pressure	6.6	bar
	Outlet absolute total pressure	25.9	bar
	Outlet absolute flow angle	69.4	°
Diffuser	Inlet static pressure	14.3	bar
	Outlet static pressure	22.7	bar
	Inlet Mach number	1.13	
	Outlet Mach number	0.30	
Compressor	Volumetric flow rate	2790	m³/h
	Impeller power	726.4	kW
	Total to total isentropic efficiency	84.8	%
	Total to total pressure ratio	3.21	

5.2 Part load CFD results

Once the design of the compressor was defined, a systematic CFD study was carried out to map the performance of the compressor, so to predict the heat pump operation at part-load. Several rotational speeds of the impeller were chosen for the simulations avoiding mechanically-forbidden ranges. For each iso-rotation speed (or speed-line), the point of lowest operation is found by lowering the flow rate until operational instabilities appear. An example of this phenomenon is shown in Figure 4(a); large recirculation areas between splitter blades and full blades of the impeller are observed and they can be

interpreted as early signs of surge. On the opposite side of a speed-line, choke can be observed (Figure 4(b)). Indeed, at high flow rates, the flow between the vaned diffuser blades enters slightly supersonic and accelerates until it is abruptly slowed down by the apparition of a nearly normal shock, which promotes separation from the pressure side of the blade. These flow rate limits deduced from CFD simulations are most likely stricter than the actual physical ones, especially for what concerns the surge limit. As a matter of fact, points to the left of the inferior flow rate boundary may lead to stable experimental operating points even if the CFD calculations show instabilities and have trouble converging to well defined solution. However, before experimental data are available, it is safer to treat these effects as early signs of surge onset.
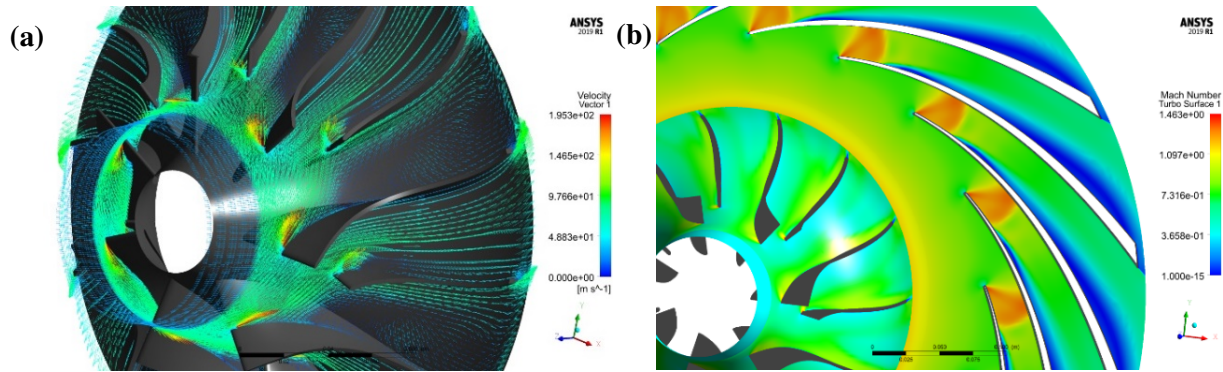

Figure 4: (a) Velocity vector field under surge conditions; **(b)** Mach number field under choke conditions

Figure 5 presents the total to total pressure ratio as a function of the volumetric flow rate for seven speed-lines. All the simulation points have been obtained using the nominal inlet total conditions of 7.2 bar and 39.7°C. This hypothesis does not represent what really happens at part load inside the heat pump because the inlet pressure and temperature depend on parameters such as the temperature of the heat source at the evaporator and the quantity of fluid inside the system. To get a more directly useful map of the compressor, a solution could be to couple the CFD simulations with a full heat pump system simulation tool. However, this solution was deemed too costly in computation time given the scope of this study. Moreover, and more importantly, the curves achieved by this approach can be made non-dimensional, and, considering that self-similarity in Reynolds number is well attained in this case (the Reynolds number based on the impeller diameter and the peripheral speed is of the order of 10^7 for the present application), they can be used to predict the compressor performance for any possible operating condition.
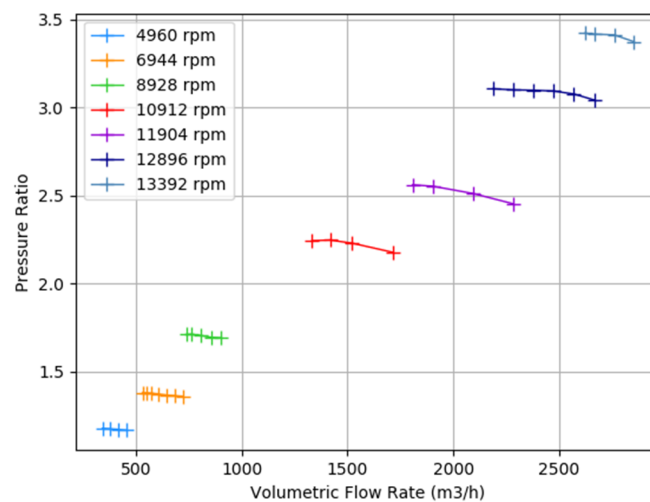

Figure 5: Off design CFD calculation results

6. EXPERIMENTAL RESULTS

6.1 Measurements

The compressor is part of an industrial plant and as such, it only beneficiates from limited measurement capacities related to the overall compressor operation. The available thermophysical sensors around the compressor are:

- Inlet pressure: single tap static pressure sensor 350 mm upstream from the IGVs
- Inlet temperature: total temperature sensor 350 mm upstream from the IGVs
- Outlet pressure: single tap static pressure sensor 300 mm downstream from the volute flange
- Outlet temperature: total temperature sensor 300 mm downstream from the volute flange
- Motor power consumption measurement

Pressure measurement accuracy is less than 0.1 bar and temperature accuracy is less than 0.35 K. No vapor flow rate measurement is available. In Figure 6(b), experimental uncertainties in pressure ratio measurement are evaluated from pressure measurement uncertainty and reported as vertical error bars.

6.2 Compressor Performance Mapping

In this industrial context, it is not possible to fully characterize the part-load performances of the compressor. Indeed, when the heat pump is running, the operating point of the compressor in terms of pressure ratio, rotation speed and power consumption is set by the control system to maximize the heat supplied to the district heating network. It is however possible to visualize part of the compressor map during start up and shut down: the curve obtained (shown in Figure 6(a)) is an intersection of the compressor's and the rest of the heat pump system's characteristics. The resulting curve is not well-defined because the control system constantly adapts for small variations of evaporator steam flow rate and district heating network temperature. However, such preliminary measurements indicate that the compressor is able to provide a pressure ratio of nearly 3 when the angular speed exceeds 12000 rpm. During the commissioning of the heat pump, when the heat source was not yet available, a test campaign aimed at partially mapping the compressor performance was carried out. The heat pump system was filled with just enough refrigerant to have a saturated liquid vapor equilibrium and used as a closed test loop for the compressor. The test procedure was the following: for each chosen rotational speed, the expansion valve was closed step by step until early signs of surge were detected. This way, we managed to change the pressure drop of the test loop and obtain different pressure ratio measurements for each speed-line. This test procedure presents several drawbacks: the pressure and temperature test conditions are far from the compressor's nominal operating point and vary during the test. Inlet pressure values were for example varying from 4.2 bar to 3.4 bar compared to the 7.2 bar nominal value. The duration of the test is also limited because the compressor constantly inputs energy into the loop and with only heat dissipation capacity the average temperature inside the system rises. For a proper comparison with CFD predictions, the mean data of the experimental conditions were recorded and subsequently used for running further CFD simulations in conditions corresponding to those of the experiments.
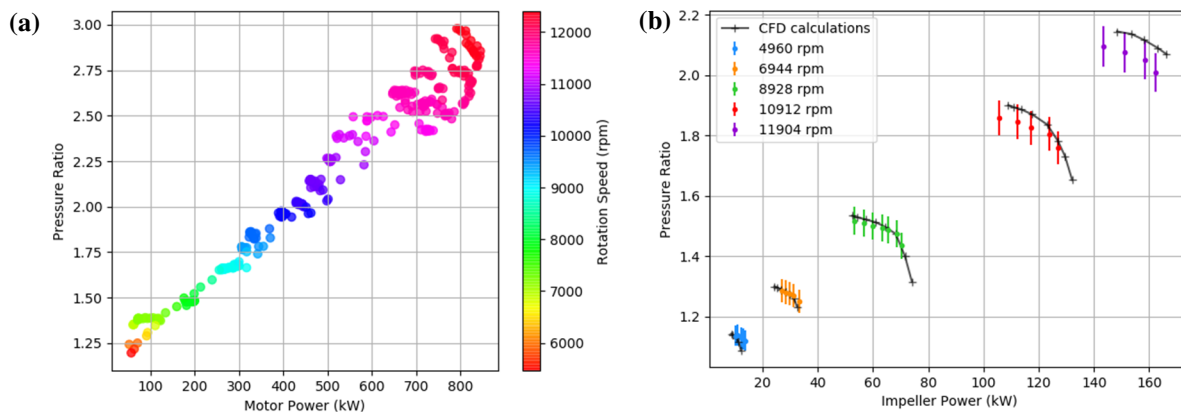

Figure 6(a): Example of a pressure ratio versus motor electrical power compressor experimental start up curve
(b): Test procedure results compared to CFD simulations (experimental uncertainties reported as error bars)

Figure 6(b) presents a comparison of the experimental data obtained and CFD simulations. For the simulation results, the impeller power is computed using the torque on the rotor blade and its angular speed. For the experimental results, the impeller power is computed from the measured motor power then applying manufacturer-supplied motor efficiency and gearbox mechanical losses. The CFD simulations seem to slightly overestimate the pressure ratio, especially at higher rotation speed; however, the computational prediction remains within the uncertainty bands of the experiments. Part of this difference may be explained by the uncertainty in the estimate of the loss in the electric motor and in the gear box at relatively low power. It is also worth noting that the pressure measurement at the inlet and outlet of the compressor are respectively upstream and downstream from the computational domain's boundaries. The effect of disc friction losses at the back of the impeller is also not taken into account.

7. CONCLUSIONS

This paper has presented the design, simulation, and test of a centrifugal compressor used in an industrial heat pump. Preliminary design tools and simplified CFD were used for design, and then 3D CFD RANS simulations of the whole machine were used to map the performance of the compressor and anticipate its operation range. The compressor's experimental behavior was analyzed during normal operation of the heat pump and during a dedicated test campaign. A good match between mean-line design predictions, CFD simulations and experimental results was shown. However, due to the industrial nature of the experimental setup, we were limited in the analysis of the experimental results. The study would beneficiate from a vapor flow rate measurement, four tap averaged pressure probes and a more direct mean of measuring mechanical power like a torque-meter. The compressor is equipped with variable IGVs at the inlet; future studies will address, applying the same type of simulations and experiments, the impact of varying the guide vane's orientation angle in spite or in combination to the impeller's rotational speed.

NOMENCLATURE

CFD	Computational Fluid Dynamics	(–)
COP	Coefficient of Performance	(–)
D	Impeller tip diameter	(m)
D_s	Specific diameter	(–)
GWP	Global Warming Potential	(–)
HFO	Hydrofluoro-Olefines	(–)
IGVs	Inlet Guide Vanes	(–)
$\dot{Q}$	Volumetric Flow Rate	(m³/s)
RANS	Reynolds-Averaged Navier-Stokes	(–)
VFD	Variable Frequency Drive	(–)
ΔH_{is}	Isentropic enthalpy rise	(J/kg)
ω	Rotational speed	(rad/s)
ω_s	Specific speed	(–)

Subscript

e	electrical
is	isentropic
s	specific
th	thermal

REFERENCES

Balje, O.E., 1981, *Turbomachines: A Guide to Design, Selection and Theory*, J. Wiley & Sons Inc.

Brown, J. S., Zilio C., Cavallini A., 2009, The fluorinated olefin R-1234ze(Z) as a high-temperature heat pumping refrigerant, *International Journal of refrigeration*, vol. 32, Issue 6, p. 1412-1422

Gaetani, P., Persico, G, Mora, A., Dossena, V., Osnaghi, C., 2012, Impeller-Vaned Diffuser Interaction in a Centrifugal Compressor at Off-Design Conditions, *ASME Journal of Turbomachinery*, vol. 134, Issue 6, 061034

Jaatinen-Varri, A., Roytta, P., Turunen-Saaresti, Gronman, 2013, Experimental study of centrifugal compressor vaneless diffuser width, *Journal of Mechanical Science and Technology*, vol. 27, Issue 4, p. 1011-1020

Khan, M. O., 1984, Best Practices in Compressor Selection, International Compressor Engineering Conference

Stoecker, W. F, 1998, *Industrial Refrigeration Handbook*, McGraw Hill

Thol, M., Lemmon, E. W., 2016, Equation of State for the Thermodynamic Properties of trans-1,3,3,3 Tetrafluoropropene [R-1234ze(E)], *Int. J. Thermophys.*, vol. 37, p.1-16.

Whitfield, A., Baines, N. C., 1990, *Design of Radial Turbomachines*, Pearson Education.